Postprint from Journal of Applied Physics 128 (2020) 045703

Lattice sites of implanted Na in GaN and AlN in comparison to other light alkalis and alkaline earths

Cite as: J. Appl. Phys. 128, 045703 (2020); doi: 10.1063/5.0009653
Submitted: 1 April 2020 · Accepted: 7 July 2020 ·
Published Online: 24 July 2020

U. Wahl,[1,2,a)] E. David-Bosne,[2] L. M. Amorim,[1] A. R. G. Costa,[2] B. De Vries,[1] J. G. Correia,[2] M. R. da Silva,[3] L. M. C. Pereira,[1] and A. Vantomme[1]

AFFILIATIONS

[1]KU Leuven, Instituut voor Kern- en Stralingsfysica, 3001 Leuven, Belgium
[2]Centro de Ciências e Tecnologias Nucleares, Departamento de Engenharia e Ciências Nucleares, Instituto Superior Técnico, Universidade de Lisboa, 2695-066 Bobadela LRS, Portugal
[3]CICECO, Institute of Materials, Universidade de Aveiro, 13810-193 Aveiro, Portugal

[a)]**Author to whom correspondence should be addressed:** uwahl@ctn.tecnico.ulisboa.pt

ABSTRACT

The lattice location of ion implanted radioactive ^{24}Na ($t_{1/2}$=14.96 h) in GaN and AlN was determined using the emission channeling technique at the ISOLDE/CERN facility. In the room temperature as-implanted state in both GaN and AlN, the majority of the sodium atoms are found on interstitial sites near the octahedral position, with a minority on cation Ga or Al substitutional sites. Following annealing at 800-900°C the interstitial fraction is reduced while the substitutional incorporation increases. Our results thus further establish the amphoteric character of Na in GaN and AlN, in analogy to the other light alkali Li, and alkaline earths Be and Mg. The site changes upon annealing are attributed to the onset of migration of interstitial Na, for which an activation energy of 2.2–3.4 eV is estimated in GaN and 2.0–3.1 eV in AlN, and its subsequent capture by cation vacancies resulting from the implantation. Comparison of the lattice site change behavior of Li, Be, Na and Mg shows that the onset of interstitial migration correlates with the ionic radii of these elements.

Published under license by AIP publishing. https://doi.org/10.1063/5.0009653

I. INTRODUCTION

Due to the widespread applications of GaN and AlN in optoelectronics, the basic properties of some key impurities in these wide band gap semiconductors have been studied quite extensively, e.g. Mg and Si as electric dopants, H as a passivating impurity, to lesser extent also rare earths for optical and transition metals for magnetic doping. For most other elements much less is known. For instance, regarding the properties of sodium, Na implantation was found to introduce a broad photoluminescence band around 2.05 eV in GaN already in 1976 [1]. However, since similar bands were observed following the implantation of other elements, this was later considered quite likely a consequence of native defects formed by the implantation damage [2]. Only a limited number of studies on Na impurities in nitrides were published afterwards, despite the fact that since 1997 liquid phase epitaxy using Na flux has been used by several groups to produce bulk GaN single crystals [3]. Comparisons of this technique to other GaN bulk growth methods can be found in a number of reviews [4-8]. In its initial implementation [9] NaN_3 was thermally decomposed into liquid Na and gaseous N_2, allowing N_2 to react with Ga dissolved in the liquid Na and thus resulting in epitaxial growth of GaN layers on GaN seed crystals. The Na metal was afterwards removed from the surface of the GaN product by reaction with ethanol. In GaN produced with upgraded Na flux techniques, traces of Na of the order of $4{\times}10^{14}$ cm^{-3} were detected [10], although also values around 10^{18} cm^{-3} have been reported [11]. The potential effects of Na incorporation in GaN are not well known. For instance, the electrical properties of Na impurities are expected to depend on their lattice sites and thus also on their ability to form complexes with other defects, e.g. in the form of Na_i^+-Mg_{Ga}^-, which would passivate Mg acceptors.

Postprint from Journal of Applied Physics 128 (2020) 045703

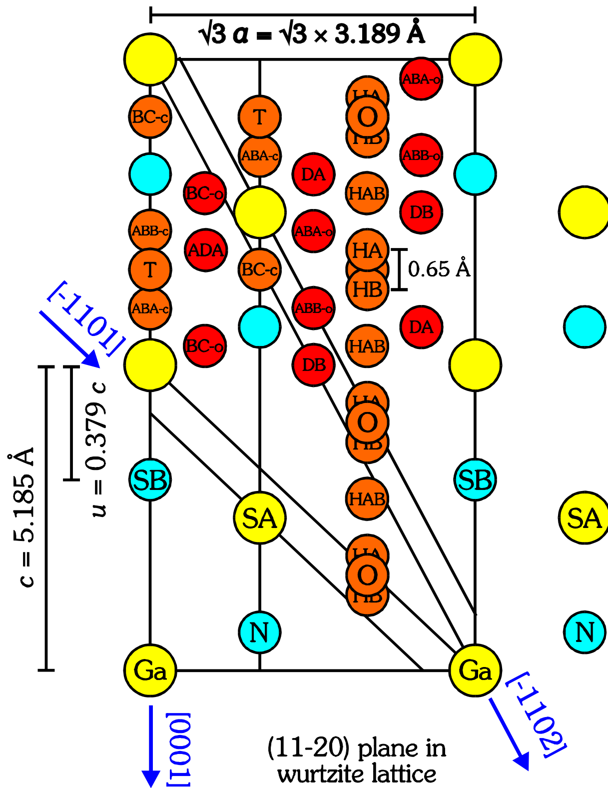

FIG. 1. The (11–20) plane of the GaN wurtzite lattice, showing the substitutional cation SA (Ga or Al) and anion SB (N) sites, as well as the following interstitial sites: bond center BC, anti-bonding AB, tetrahedral T, symmetric co-planar with Ga-N bonds D and AD, hexagonal H, and octahedral O. The addition of "A" or "B" to the site name indicates non-equivalent sites closer to the cation A or the anion B, respectively, e.g. the hexagonal sites HA and HB. On the other hand, the interstitial T, O and HAB sites are defined as having the same distance from A and B sites (i.e. located exactly at the center in between planes of A and B atoms). "-c" indicates BC or AB sites located within the atomic rows along the *c*-axis, while those indicated with "-o" are basal to it. The directions around which the β^- angular emission yield from ^{24}Na was measured are represented by the vectors shown in blue. The values indicated for the lattice constants *a* and *c* as well as for the bond length parameter *u* are those of GaN. A sketch showing the (01–10) plane, which includes the [–2113] axis that was also measured, can be found in the supplementary material.

A first-principles theoretical investigation of the potential acceptor impurities Li, Na, K, Be and Mg in GaN [12] predicted that for the light alkali metals Na and Li interstitial Na_i and Li_i exhibit lower energies of formation than substitutional Na_{Ga} and Li_{Ga} as long as the Fermi level is below ~1.2 eV and ~1.7 eV, respectively, with respect to the valence band. This means that, in thermodynamic equilibrium, in *p*-type GaN the incorporation of Na and Li impurities on interstitial sites, where they act as single donors, should be more favorable than on the substitutional Ga site, where they represent double acceptors. In contrast, in *n*-type GaN, the predominant Na and Li species should be substitutional Na_{Ga} and Li_{Ga}. The interstitial positions considered by theory were the octahedral (O) and tetrahedral (T) sites, with the octahedral site predicted to be more favorable [12]. As can be seen from Fig. 1, T sites are interstitial sites aligned with the *c*-axis, while O sites are located within the open "channels" of the wurtzite structure parallel to the *c*-axis, both T and O sites are located exactly at the center in between planes of A and B atoms. A recent theoretical study addressed the detailed positions of interstitial Mg, Be, Li, and Na in GaN, as well as their migration paths and related migration energies [13]. It was predicted that the most stable position for interstitial Na^+ is "0.28 Å from ideal octahedral sites". In that respect it must be noted that the definition of ideal O sites in Ref. [13] is different from the one used by us and, for instance, Refs [14-15]; the location of the "ideal O site" in Ref. [13] corresponds to our HA site (which is located at $+c/16$=+0.324 Å from O). Hence the Na^+ site coordinate predicted by Ref. [13] is in our nomenclature at +0.04 Å from O towards HA sites, thus very close to the ideal O site.

The lattice location of radioactive ^{24}Na implanted in GaN and AlN was investigated by Ronning *et al.* [16] using the β^- emission channeling technique. Following 30 keV room temperature implantation of ^{24}Na at a fluence of $2{\times}10^{13}$ cm^{-2} into GaN and AlN, ~40-44% of Na was found aligned with the *c*-axis rows in both cases, while ~56-60% was located on interstitial sites off the *c*-axis. The interpretation was that all of the Na that were found aligned with the *c*-axis occupied substitutional sites (which could be cation or anion sites), while the interstitial positions off the *c*-axis were assumed to be O sites, although no definite proof could be given. Only experimental channeling patterns around the [0001] axis were compared to simulated yields for different lattice sites; [−1101] patterns were measured but not analyzed in detail. However, for assessing exact positions along the *c*-axis or parallel to it, which is required for instance in order to properly distinguish between the cation and anion substitutional sites and the interstitial T sites, or in order to quantify the displacement from interstitial O sites parallel to the *c*-axis, the analysis of patterns off the *c*-axis is required. The exact locations of substitutional and interstitial Na could hence not be pinpointed in Ref. [16]. Annealing at 800°C for 10 min was reported to relocate part of the interstitial Na to sites aligned with the *c*-axis in AlN, while the same treatment seemed to have no effect on ^{24}Na in GaN.

In this article we report on detailed measurements of the lattice location of implanted ^{24}Na in GaN and AlN, in the room temperature (RT) as-implanted state and for annealing temperatures up to 900°C. In addition to [0001] (*c*-axis) emission channeling patterns, also [−1102], [−1101], and [−2113] directions off the *c*-axis were measured. Fitting all the experimentally observed electron yield distributions to theoretical patterns calculated for a variety of lattice sites, aligned and off the *c*-axis, allowed

Postprint from Journal of Applied Physics 128 (2020) 045703

determining the location of interstitial Na within ~0.2 Å. Moreover, lattice site changes of Na from interstitial to substitutional sites that were observed following annealing in both GaN and AlN, allowed deriving estimates for the Na interstitial migration energies. Finally, we compare the lattice location preference of Na and its interstitial diffusion characteristics to the corresponding properties of Li, Mg, and Be, pointing out qualitative similarities and systematic quantitative differences.

II. METHODS

β^- emission channeling is a nuclear technique that allows measuring the lattice location of radioactive impurities implanted in a single-crystal [17-19]. The β^- particles emitted during the decay of radioactive probe atoms travel inside the crystal with enough energy to perceive the nuclei arranged along axes and planes as a positive continuum potential that is formed by the average of individual, screened Coulomb potentials. Thus, in a simplified view, the negatively charged β^- particles that are emitted from sites that are aligned with high symmetry axes or planes of the crystal, e.g. from substitutional sites, are channeled if the emission occurred within certain critical angles, while those emitted above the critical angle are scattered randomly. On the other hand, emission from interstitial sites that are not aligned with crystallographic axes or planes generally leads to enhanced scattering along these directions. Using a two-dimensional position-sensitive detector (PSD) which is successively oriented with the major axial directions of the crystal, the angular emission yield around these axes is measured, which is a characteristic of the probe atom lattice location in the sample. The two-dimensional angular emission yields are fitted with linear combinations of simulated patterns of emitter atoms on different lattice sites.

For lattice location of Na, we made use of the same radioactive isotope ^{24}Na ($t_{1/2}$=14.96 h) as in Ref. [16]. The production of ^{24}Na at the on-line isotope separator facility ISOLDE/CERN [20] as well as its relevant decay characteristics have been outlined in our previous publication on the lattice location of ^{24}Na in ZnO [21]. The experimental setup is described in Ref. [22]. All samples were measured using Si pad PSDs consisting of 22×22 pixels of size 1.3 mm, our standard systems for electron emission channeling studies [23]. The GaN sample #1 (cf. Table I) was in addition studied with a new, highly pixelated quad Timepix PSD consisting of 512×512 pixels of 55 µm size [24-25], thus allowing to compare the results from two different measurement and analysis methods. Both detectors were mounted at a distance of 30 cm from the sample, leading to angular resolutions of 0.081° (standard deviation) for the pad geometry and 0.050° for the Timepix. Note that for the pad detector the size of the 1 mm diameter beam spot on the sample and the detector pixel size of 1.3 mm contribute with comparable magnitude to the angular resolution, while for the Timepix detector, the angular resolution is dominated by the beam spot dimension [26].

TABLE I. Samples, implantation and measurement parameters. All samples were implanted at RT and measured in the as-implanted state and following 10 min annealing under vacuum at the indicated temperatures T_A. See Ref [29] for additional sample properties.

Sample	GaN #1	GaN #2	AlN
Growth method	MOVPE (U Cambridge)	MOVPE (Cree Inc.)	MOVPE (U Montpellier)
Film thickness (µm)	4.8	1.5	0.28
Implantation energy (keV)	40	50	60
Implantation angle (°)	17	10	10
Fluence (cm^{-2})	2.9×10^{13}	4.8×10^{12}	5.3×10^{12}
Projected range (Å)	422	535	825
Straggling (Å)	209	257	300
[^{24}Na]$_{peak}$ (cm^{-3})	4.9×10^{18} (55 ppm)	6.2×10^{17} (7 ppm)	6.9×10^{17} (7 ppm)
T_A (°C)	800	900	600, 900
Detector	pad + Timepix	pad	pad

The “many-beam” theoretical approach for calculating electron emission channeling patterns from emitter atoms on different lattice sites has been discussed in Refs [17-18] and input parameters for the structural models of GaN and AlN are given in Refs [27-28]. The fit routines for comparing experimental and theoretical data were outlined in Refs [18, 23] and recently described in detail in Ref. [26]. For fitting the results obtained with the pad detector we used our proprietary software FDD, while Timepix patterns were fitted using the newly developed PyFDD code, in both cases using chi square minimization [26]. The fitted fractions were corrected for background from scattered electrons and from gammas, as is explained in more detail in Refs [21, 29].

Three samples (two GaN and one AlN, all not intentionally doped) were implanted using the parameters given in Table I, with beam spots of 1 mm diameter. While the GaN samples were 1.5 and 4.8 µm thick layers grown on sapphire, the AlN sample [30] consisted of a 0.28 µm AlN thin film with a 0.55 µm $Al_{0.2}Ga_{0.8}N$ buffer layer on a sapphire substrate. It is known that AlN films are subject to suffer from more structural imperfections and mosaicity than GaN. Hence the tilt and twist values of the mosaic domain distributions for this AlN sample were determined

Postprint from Journal of Applied Physics 128 (2020) 045703

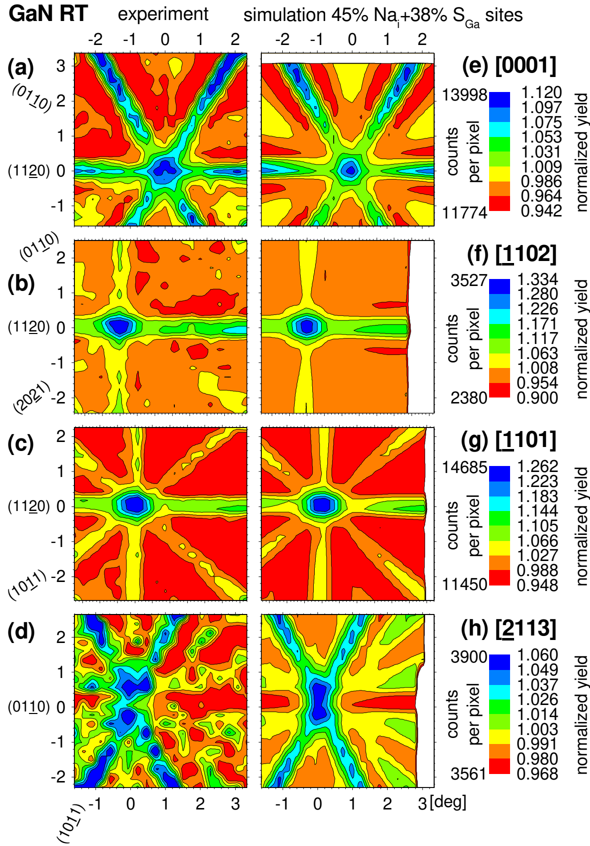

FIG. 2. (a)-(d) Angular distribution of β⁻ emission yields from ^{24}Na in GaN sample #1, measured as-implanted at RT with the pad detector. Patterns are shown as contour plots around the [0001], [−1102], [−1101] and [−2113] axes, with the color scales indicating both number of counts per pixel and the normalized yields. The approximate numbers of events measured were 6.0×10^6 (a), 1.6×10^6 (b), 6.9×10^6 (c), and 2.1×10^6 (d). (e)-(h): the best fit of simulated patterns, corresponding to 45(8)% on Na$_i$ interstitial and 38(4)% on S$_{Ga}$ sites.

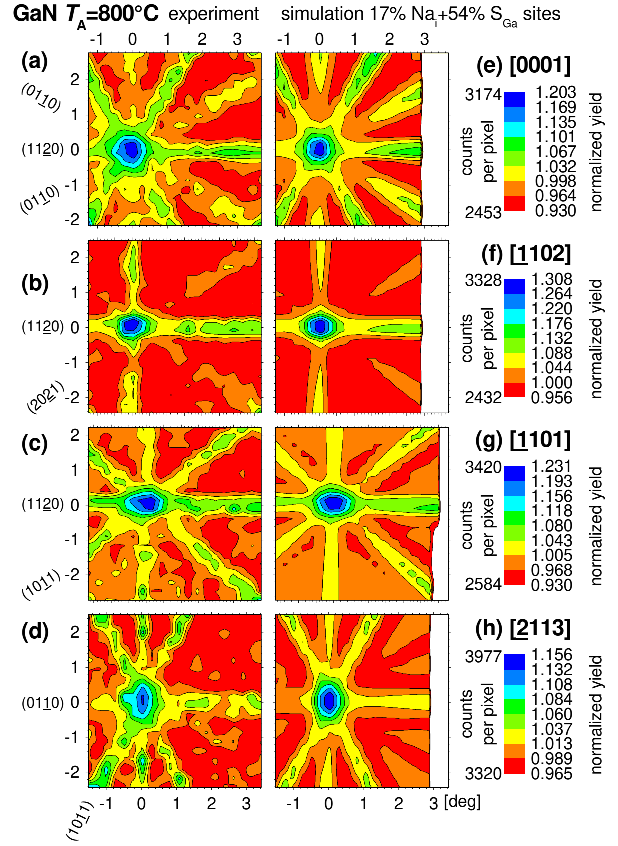

FIG. 3. Same as Fig. 2 but measured following annealing at T_A=800°C. (a)-(d) are experimental patterns while (e)-(h) show the best fit of simulated patterns, corresponding to 17(2)% on Na$_i$ interstitial and 54(5)% on S$_{Ga}$ sites. The approximate numbers of events measured were 2.0×10^6 (a), 1.5×10^6 (b), 1.3×10^6 (c), and 1.3×10^6 (d).

by means of X ray diffraction using the method of Srikant et al. [31-33], and values of W_{tilt}=0.20° and W_{twist}=0.56° were found [29] (in contrast, typical values for GaN samples are around W_{tilt}≈0.1° and W_{twist}≈0.10-0.20° [29]). The tilt and twist values were taken into account by adjusting the angular resolution of the theoretical patterns used for the fits, as described in Ref. [32]. The angular emission yields in the vicinity of the four high-symmetry directions [0001], [−1102], [−1101] and [−2113]) were measured at RT, both in the as-implanted state and following 10 min vacuum annealing steps as indicated in Table I.

III. RESULTS

A. Best fit patterns

The experimental emission channeling patterns measured as-implanted in GaN with the pad detector are plotted in Fig. 2(a)-(d). Simulated patterns resulting from ^{24}Na radioactive probes in GaN on a number of different lattice sites are shown in the supplementary material. While the yield maximum measured along the [0001] axis [in the center of Fig 2(a)] is a characteristic of probes on substitutional (S) or tetrahedral (T) interstitial sites, which are all aligned with the *c*-axis, the planar emission yields in the same pattern show major channeling effects only along the set of three (11−20) planes, while the channeling yields from the set of three (01−10) planes are considerably reduced. In the wurtzite structure this combination of planar effects is a strong indication that, besides sites aligned with the *c*-axis, a large fraction of probe atoms occupies sites in the wide open interstitial region of the lattice parallel to the *c*-axis [21]. This is further evidenced by the characteristics of the [−2113] pattern: while substitutional ^{24}Na alone would create strong (01−10) planar channeling along the "horizontal plane" in Fig. 2(d), ^{24}Na near the interstitial O sites results in "blocking" along the same plane. In the case of [−1102] and [−1101] directions the distinction between octahedral interstitial and substitutional ^{24}Na is not immediately obvious since

Postprint from Journal of
Applied Physics 128 (2020) 045703

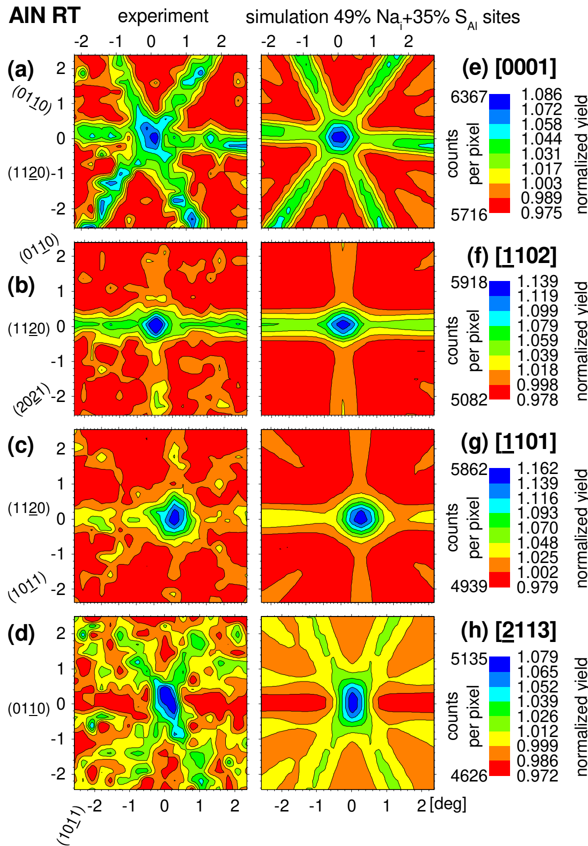

FIG. 4. (a)-(d) Angular distribution of β⁻ emission yields from ^{24}Na in AlN, measured as-implanted at RT with the pad detector. Patterns are shown as contour plots around the [0001], [−1102], [−1101] and [−2113] axes. The approximate numbers of events measured were 3.2×10^6 (a), 2.9×10^6 (b), 2.9×10^6 (c) and 2.7×10^6 (d). (e)-(h): the best fit of simulated patterns, corresponding to 49(15)% on Na_i interstitial and 35(6)% on S_{Al} sites.

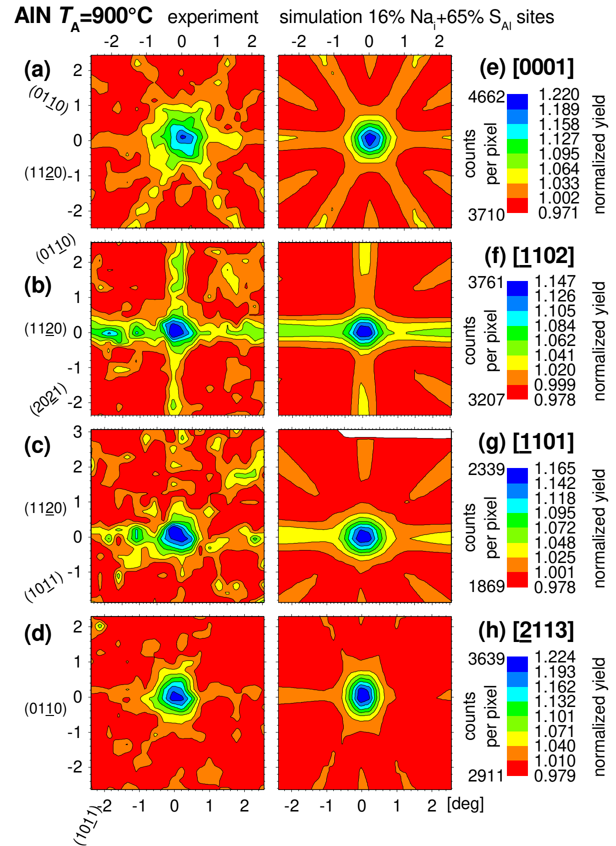

FIG. 5. Same as Fig 4 but measured following annealing at T_A=900°C. (a)-(d) are experimental patterns while (e)-(h) show the best fit of simulated patterns, corresponding to 16(10)% on Na_i interstitial and 65(8)% on S_{Al} sites. The approximate numbers of events measured were 2.4×10^6 (a), 2.2×10^6 (b), 2.0×10^6 (c) and 2.6×10^6 (d).

the O sites are approximately aligned with these axial directions (cf. Fig. 1). The results of fitting a linear combination of theoretical patterns from ^{24}Na probes on two different lattice sites fully confirmed the qualitative arguments outlined above: the best fits [Fig. 2(e)-(h)] were obtained for fractions of 38(4)% of ^{24}Na on S_{Ga} and 45(8)% very close to the octahedral interstitial O sites. The difference of the sum of the two fractions from 100% is assigned to the so-called “random” fraction, that results from a flat background in the patterns and e.g. includes probe atoms in sites of very low crystal symmetry [26]. Note that the positions of the interstitial Na_i sites parallel to the *c*-axis used for Fig. 2(e)-(h) were identified as described below in section B.

Following 800°C annealing, several features in the measured patterns changed [Fig. 3(a)-(d)]. In the [0001] pattern [Fig. 3(a)], the axial channeling effect almost doubled in intensity, and channeling effects from both (11−20) and (01−10) planes are now clearly visible. In the [−2113] pattern, the axial channeling effect, which was characterized in the as-implanted state by a double peak of low intensity, turned into a much stronger single peak, at the same time the (01−10) plane changed from blocking to channeling. These qualitative arguments indicate that interstitial ^{24}Na was converted to substitutional, which was confirmed by the best fits [Fig. 3(e)-(h)], which were obtained for fractions of 54(5)% of ^{24}Na on S_{Ga} and only 17(2)% on the octahedral interstitial O sites. The experimental results and best fit patterns measured for the same sample GaN #1 with the Timepix detector and for GaN #2 with a pad detector can be found in the supplementary material [29].

The patterns measured for ^{24}Na in AlN are shown in Fig. 4(a)-(d) in the as-implanted state and in Fig. 5(a)-(d) following the last annealing step at 900°C. Due to the lower structural quality of the AlN sample, but also a number of other reasons [29], the patterns show less contrast than GaN. However, the axial and planar features that allow distinguishing the preference for interstitial sites of ^{24}Na in the as-implanted state and for substitutional Al sites following annealing, are also present. The best fits were

**Postprint from Journal of
Applied Physics 128 (2020) 045703**

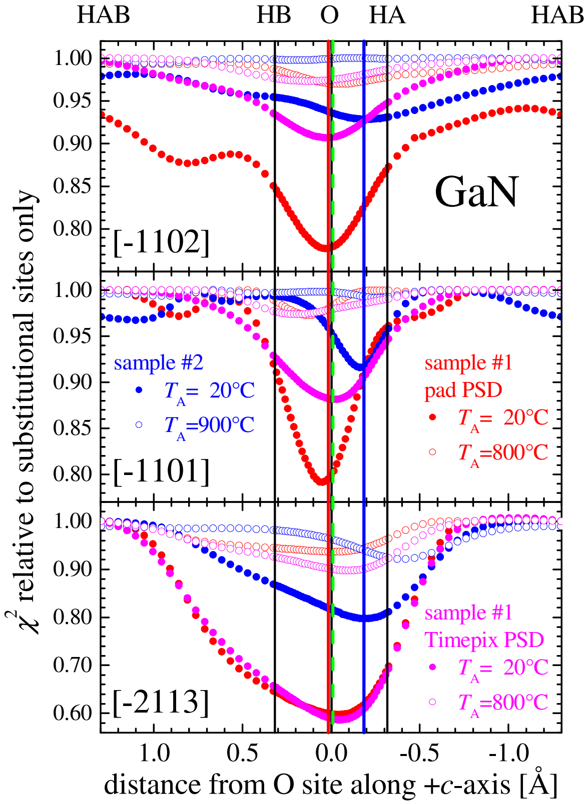

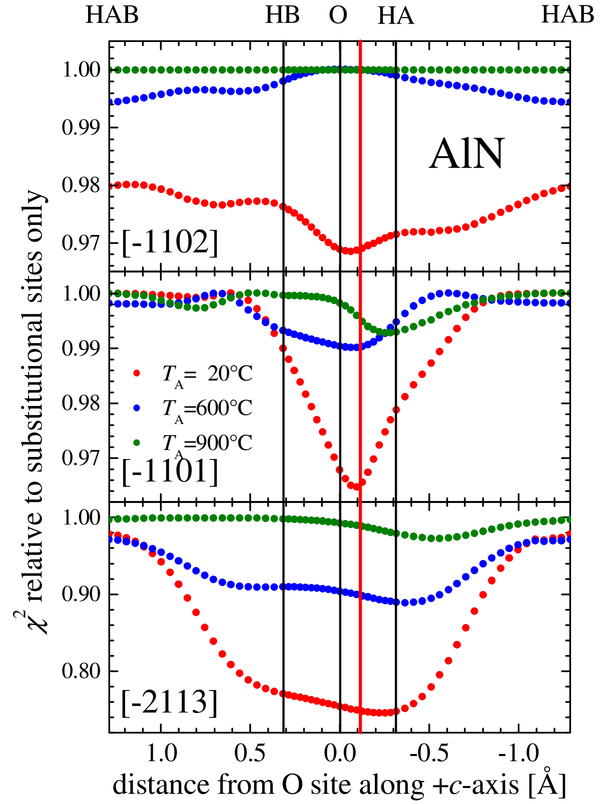

FIG. 6. Relative χ^2 of the fits to the experimental [–1102], [–1101], [–2113] patterns from ^{24}Na in GaN as function of displacement of the ^{24}Na atoms from the ideal interstitial O sites parallel to the *c*-axis. Each data point corresponds to the χ^2 of the best fit obtained using two given sites, with the corresponding two fractions as free parameters. The site pairs are composed of a fixed S_{Ga} site plus a second site, which is shifted from the ideal interstitial O site along the *c*-axis. The relative χ^2 values were normalized to that of the one-site S_{Ga} fit. The black vertical lines indicate the positions of the HB, O and HA interstitial sites. The dashed green line is the theoretically predicted position of Na_i^+ in GaN from Ref. [13], which practically coincides with the O site. The red vertical line shows the average of the best fit positions from sample #1, while the blue vertical line shows the average from sample #2, both in the as-implanted state.

FIG. 7. Relative χ^2 of the fits as function of ^{24}Na displacement from the ideal interstitial O sites parallel to the *c*-axis in AlN. Normalization is as described in the caption of Fig. 8. The red vertical line shows the average of the best fit positions in the as-implanted state. The [-1102] fits following T_A=600°C did not result in chi square minima consistent with the other directions, and following annealing at T_A=900°C yielded negative interstitial fractions (which we have represented by the straight line at 1.0). In both cases chi square changes were so small that [-1102] patterns following annealing could actually not be used for determining the interstitial position.

obtained for 49(15)% on Na_i interstitial and 35(6)% on S_{Al} sites as-implanted [Fig. 4(e)-(h)], and 16(10)% on Na_i interstitial and 65(8)% on S_{Al} sites following T_A=900°C [Fig. 5(e)-(h)].

B. Positions of Na_i interstitial sites

In order to determine as accurately as possible the most probable positions of interstitial ^{24}Na parallel to the *c*-axis, i.e. to distinguish between the octahedral (O) and various hexagonal interstitial sites (HA, HB and HAB), schematically shown in Fig. 1, we have applied the following procedure to the [–1102], [–1101] and [–2113] patterns (channeling effects measured along [0001] are not sensitive to displacements parallel to the *c*-axis). Note that in contrast to our former publications [19, 21, 26, 28, 34], we have now adopted that displacements from O to HB sites are represented by a positive coordinate, since they occur along the +*c*-axis [0001] (cf. Figs 1, 6 and 7), while displacements from O to HA are associated with negative coordinates, since they occur along –*c*-axis [000–1]. This was chosen so as to be in line with the convention used in other publications, e.g. [13-15]. In Figs 6 and 7 the relative χ^2 is plotted for two-site fits where the position of the first site is kept fixed at the ideal substitutional Ga or Al site, while the position of the second site is varied parallel to the *c*-axis in small steps of 0.016 Å from O to HA or HB, and 0.049 Å from HA to HAB and HB to HAB. Note that χ^2 is given relative to one-site fits that include only the ideal substitutional site. For as-implanted ^{24}Na in GaN sample #1 (red curves in Fig. 6) the relative χ^2 for the [–1102], [–1101] and [–2113] pad detector pattern fits shows minima for interstitial sites which are displaced by

Postprint from Journal of Applied Physics 128 (2020) 045703

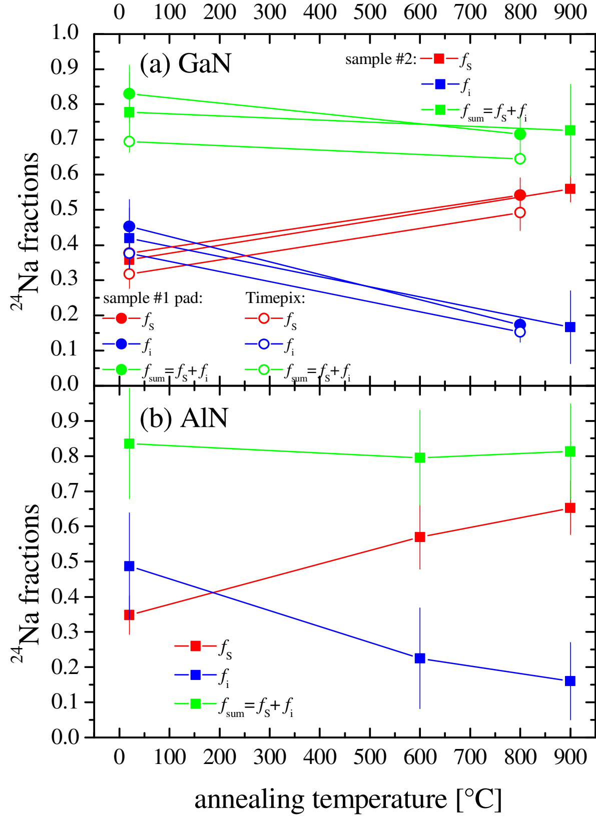

FIG 8. ^{24}Na in GaN (a) and AlN (b): Fractions on substitutional Ga or Al (f_S) and near octahedral interstitial O (f_i) sites, as well as the sum of both (f_{sum}). The error bars reflect the spread in fractions derived from the patterns of the four crystallographic directions measured at each temperature.

+0.032 Å, +0.049 Å, and −0.032 Å from ideal O sites, with the average of the three derived displacements being +0.016 Å, i.e. very close to the ideal O sites. The identical type of analysis performed for the patterns measured for the same sample #1 with the Timepix detector (magenta curves in Fig. 6), yields displacements of +0.016 Å, −0.016 Å, and −0.049 Å from ideal O sites, average value −0.016 Å. The two separate measurement and analysis procedures hence agree on the result that interstitial ^{24}Na is found very close to ideal O sites in sample #1. However, the same kind of analysis showed somewhat different results for the GaN sample #2 (blue curves in Fig. 6), the relative χ^2 for the [−1102], [−1101] and [−2113] pattern fits shows minima for Na_i interstitial sites displaced −0.194 Å, −0.162 Å, and −0.194 Å from ideal O sites, with the average being −0.184 Å, hence closer to HA than to O sites. Following annealing, the variations in χ^2 are much less pronounced for both GaN samples, also the spreads in between the minima of the best fit positions become larger, both due to the fact that the fractions of interstitial ^{24}Na are considerably reduced, causing the statistical relevance of the results to be less significant and the assessment of the Na_i interstitial position to be less precise.

In case of AlN the relative χ^2 for the [−1102], [−1101] and [−2113] pattern fits (Fig. 7) shows minima for interstitial sites displaced −0.063 Å, −0.095 Å, and −0.221 Å from ideal O sites, with the average being −0.126 Å. Overall, the relative changes in χ^2 as a function of the position of the interstitial Na_i site are less pronounced in AlN than in GaN. We attribute this to the larger mosaic spread of the AlN film, which effectively lowers the angular resolution of the channeling measurements and hence also diminishes the ability to distinguish different lattice sites.

C. Substitutional and interstitial fractions

Figure 8 shows the fractions f_S and f_i of ^{24}Na on susbstitutional and interstitital lattice sites, as well as the sum f_{sum}=f_S+f_i of both, as a function of annealing temperature. The general picture is that in the as-implanted state interstitial sites dominate over substitutional ones, while following annealing at 800-900°C, the interstitial fraction is greatly reduced in favour of the substitutional one, hence that site changes of Na took place. The 600°C annealing results for AlN show that this site change already partly happened at this lower annealing temperature. The scatter in the fractions derived for the GaN sample #1 from pad and Timepix detector measurements is within the expected range of precision of our technique, where errors of ±10% in sum fractions f_{sum} are expected, due to the limited accuracy of background corrections for different measurement conditions [26]. We also performed 3-site fits where the first two sites were kept fixed at the substitutional Ga or Al site and the identified Na_i positions near the O site, while the third site was varied over the whole range of sites calculated. However, this did not result in significant and consistent improvements in fit quality. One may hence conclude that additional lattice sites could not be identified, in particular no Na was found on substitutional N or interstitial T sites.

IV. DISCUSSION

Our results fully confirm the co-existence of ^{24}Na near interstitial O and substitutional cation positions following RT implantation into GaN and AlN, as was sugested by Ronning *et al.* [16] on the basis of less detailed data. We also confirm the partial site change they reported for ^{24}Na in AlN following annealing at 800°C. In addition, we were able to show the partial site change in GaN following 800-900°C annealing, which was not obvious in the experiments of Ronning *et al.*

Also in contrast to previous measurements [16], we were able to determine the positions of interstitial ^{24}Na parallel to the *c*-axis. In GaN sample #1 we found within measurement accuracy the interstitial Na exactly at the O site, as predicted by theory [13]. However, in sample #2 the

Postprint from Journal of Applied Physics 128 (2020) 045703

derived ^{24}Na position was −0.18 Å off the O site, hence located closer to the HA site. While these different assessments could be due to limitations in the accuracy of our lattice location method, the fact that the displacements derived from all three off-surface directions of each sample are rather consistent, suggests that the ^{24}Na lattice sites might in fact differ by ~0.2 Å in between both samples (a more detailed discussion can be found in the supplementary material). The major known differences of the two samples are the implanted fluence (2.9×10^{13} cm^{-2} for sample #1 *vs* 4.8×10^{12} cm^{-2} for sample #2) and a smaller mosaic spread for sample #1 [29], resulting from the use of a more advanced growth technique. Due to the extraordinary radiation hardness and dynamic annealing of GaN and AlN, no major effects of implantation damage are expected for the fluence range used in our experiments. For instance, for ^{28}Si RT implantations in GaN, no detectable damage could be observed with Rutherford Backscattering Spectrometry/Channeling (RBS/C) for fluences up to 10^{14} cm^{-2} [19, 35], the same applies to 10^{14} cm^{-2} ^{24}Mg implantations investigated by X-ray diffraction [36]. In case of AlN, for 6×10^{13} cm^{-2} ^{40}Ar implantations performed at 15 K hardly any damage was visible by RBS/C [37]. Since the apparent slight shift of ~0.2 Å is close to the expected precision of our experiments [29], in order to proof this difference is real, more experiments with larger numbers of equivalent samples would be required, thus reducing statistical spreads.

In both GaN and AlN, annealing at elevated temperature induced site changes of interstitial Na to substitutional cation sites. We interpret these site changes as resulting from the onset of migration of interstitial Na_i^+ which then may combine with Ga or Al vacancies created during the implantation process. Similar behavior has been previously observed in emission channeling lattice location experiments following the implantation of the light alkali metal ^{8}Li in a large number of III-V and II-VI semiconductors including e.g. GaAs [38], GaP [38], InP [38], InSb [38], GaN [16, 39], and AlN [16]. In case of ^{8}Li in GaN and AlN the site changes from interstitial to substitutional cation sites took place at a temperature around 700 K, corresponding to ~427°C. As we have previously reported, similar site change effects have also been observed following the implantation of ^{27}Mg in GaN [19, 26, 34] and AlN [28]. On the other hand, emission channeling studies with ^{45}Ca [40] and ^{89}Sr in GaN [16, 40] identified only substitutional Ga sites while finding no indications of interstitial fractions for these heavier alkaline earths. One may therefore conclude that in GaN and AlN the co-existence of interstitial and substitutional sites, hence an amphoteric nature, seems to be a characteristic of the light alkali and alkaline earth metals, which all have been studied for use as *p*-type dopants in GaN [2, 12-15]. Establishing the amphoteric nature of these elements hence improves our understanding why *p*-type doping is not possible at all (e.g. using Be), or limited in its efficiency, as is the case for Mg, the only technologically feasible *p*-type dopant of GaN.

By making some simple assumptions for the number of jumps N which are needed for the interstitial ^{24}Na impurity until it combines with a vacancy, it is possible to derive estimates for the activation energy of interstitial migration E_M from the temperatures T where the site changes occur and the duration of the annealing Δt_{ann}. The mathematical formula appropriate for the case of ^{24}Na (simple Arrhenius model, implantation of long-lived radioisotope at room temperature, subsequent isochronous 10 min annealing steps) has been given in Ref. [21] as

$$E_{\mathrm{M}} = k_{\mathrm{B}} T \ln\left[\frac{\nu_0 \Delta t_{\mathrm{ann}}}{N \ln(f_{\mathrm{i0}}/f_{\mathrm{i}})}\right]$$

where ν_0 is the attempt frequency, N the number of jumps, and f_{i0} and f_i the interstitial fractions before and after each annealing step. We have assumed $\nu_0=10^{12}$ s^{-1}, and N to range from N=1 (cation vacancy and interstitial Na_i are next neighbours) to N≈200000 (diffusion width corresponds to mean implantation depth). This results in estimated values of E_M≈2.2−3.4 eV for GaN and E_M≈2.0−3.1 eV for AlN.

In Table II we have compiled the experimentally observed temperatures $T_{i\rightarrow S}$ of the site changes for Li, Na and Mg in GaN and AlN and the corresponding estimates for the migration energies $E_{M,exp}$ and compared them to theoretical predictions for E_M from the literature. In case of the alkaline earth Be in GaN, preliminary results indicate the co-existence of substitutional and interstitial ^{11}Be at room temperature, with the major site change taking place around 350-400°C [42]. As a general rule, both in GaN and AlN, $T_{i\rightarrow S}$ is lowest for Mg, followed by Li and highest for Na, with all site changes in AlN occurring at lower temperatures than in GaN. Since Li and Na are more volatile metals than Mg, naively one might expect that Li and Na change sites at lower temperatures than Mg. However, when comparing the ionic radii of Li^+, Na^+ and Mg^{2+} one concludes that the temperatures of the site changes correlate with the ionic radii of the likely charge states of the interstitials, which are 1+ for alkalis and 2+ for alkaline earths. Such a correlation was also predicted by theory [13]. A surprising fact is that the temperatures of the site changes are generally lower in AlN than in GaN. Since AlN has a greater bond strength and hence a more rigid lattice than GaN, which should hinder diffusion, this observation has no simple explanation. We also note that the interstitial diffusion of Na in ZnO is much faster than in GaN, with Na site changes in ZnO happening already around 145°C (cf. Table II), although the two materials have quite similar structural properties.

Postprint from Journal of Applied Physics 128 (2020) 045703

TABLE II. Comparison of the characteristics for the site changes of light alkalis and alkaline earths in GaN, AlN and ZnO. $T_{i\rightarrow S}$ is the temperature of the site changes from interstitial to substitutional Ga, Al or Zn sites observed in emission channeling experiments following the implantation of the radioactive isotopes ^{8}Li ($t_{1/2}$=838 ms), ^{11}Be ($t_{1/2}$=13.8 s), ^{24}Na ($t_{1/2}$=14.96 h) and ^{27}Mg ($t_{1/2}$=9.45 min). The characteristic time scales Δt for the site changes are the radioactive lifetimes τ in case of the short-lived isotopes ^{8}Li (τ=1.2 s), ^{11}Be (τ=19.9 s) and ^{27}Mg (τ=13.6 min), but a fixed annealing time of 10 min in the case of ^{24}Na. $E_{M,exp}$ are the experimental estimates for the activation energies for migration of the interstitial impurities derived from $T_{i\rightarrow S}$, while $E_{M,theo}$ are values predicted by theory, with (⊥) indicating values for migration perpendicular and (‖) parallel to the *c*-axis. The ionic radii given are the so-called "crystal ionic radii" for 4-fold coordination from Ref. [41].

Material	Interstitial ion	Ionic radius (Å)	$T_{i\rightarrow S}$ (°C)	$E_{M,exp}$ (eV) [Ref]	$E_{M,theo}$ (eV) [Ref]
GaN	Li^{+}	0.76	~427	~1.7 [16, 39]	1.4 (⊥) 1.55 (‖) [43], 1.16 (⊥) 1.05 (‖) [13]
	Be^{2+}	0.41	350–400	1.2–2.1[a] [42]	1.2 (⊥) 2.9 (‖) [14], 0.76 (⊥) 1.88 (‖) [13]
	Na^{+}	1.13	~900	2.2–3.4 [this work]	2.95 (⊥) 2.41 (‖) [13]
	Mg^{2+}	0.71	~400	1.3–2.0 [34]	0.15 (⊥) 0.68 (‖) [44-45], 2.20 (⊥) 2.01 (‖) [13]
AlN	Li^{+}	0.76	~427	~1.7 [16]	
	Na^{+}	1.13	600–900	2.0–3.1 [this work]	
	Mg^{2+}	0.71	300–400	1.1–1.7 [28]	
ZnO	Na^{+}	1.13	~145	0.81–1.32 [21]	0.74 (⊥) 1.33 (‖) [46]

[a] Based on a preliminary analysis of recent ^{11}Be lattice location measurements [45], the major site change of Be occurs around 350-400°C, but there may be further contributions at higher and lower temperatures.

Comparing the experimental estimates $E_{M,exp}$ to the theoretical predictions for E_M, as shown in Table II, one concludes that there is usually good correspondence. An exception are the values of 0.15 eV and 0.68 eV predicted by Harafuji *et al.* [44-45] for migration of Mg in GaN perpendicular and parallel to the *c*-axis, which are by far too low to be compatible with the experimental estimate of 1.3–2.0 eV of Ref. [33] and also do not scale well with all other theoretical predictions in Table II.

Macroscopic diffusion studies for light alkali and alkaline earth elements in GaN at temperatures around 900–1500°C give a somewhat disperse picture. While no data are available for Li and Na, for Be in GaN an activation energy for macroscopic diffusion of ~4 eV was reported [47]. In the case of the major *p*-type dopant Mg in GaN, several studies found no or very little diffusion [48-49], while others claim quite low activation energies, e.g. 1.3 eV [50] and 1.9 eV [51]. While low activation energies for Mg diffusion have often been associated with diffusion along dislocation lines [52-53], the emission channeling results suggest that in the absence of traps such as vacancies also simple interstitial diffusion should play a significant role. A carefully analyzed study led to the conclusion that macroscopic Mg diffusion in GaN occurs by the interstitial-substitutional mechanism with an activation energy of 5.0 eV [54]. We note that an interstitial-substitutional diffusion mechanism is also what one would expect taking into account the emission channeling results showing the high interstitial diffusivities of Li, Be, Na and Mg. The activation energy for macroscopic diffusion is in this case essentially the same as the activation energy for the dissociation of the substitutional impurity, E_{diss}. Using positron annihilation spectroscopy, the creation of Ga vacancies in Be-doped GaN has recently been observed following prolonged (2 h) annealing at 900°C [55]. The corresponding activation energy was derived as E_{diss}=3.5 eV, which roughly coincides with the activation energy for macroscopic Be diffusion of 4.0 eV reported in Ref. [47]. It has not been possible to directly determine E_{diss} of substitutional Li, Be, Na and Mg in GaN and AlN using emission channeling, since our experimental setups are limited to 800-900°C annealing and thus can only reach the lower limit of the required temperature range. Note that we did not attempt to explore the Fermi level effect on substitutional *vs* interstitial Na preference predicted by theory [12], since implantations above 1×10^{12} cm^{-2} already seem to push the *p*- or *n*-doping type of GaN towards intrinsic conditions [19, 34].

V. CONCLUSIONS

Emission channeling studies of the lattice location of implanted ^{24}Na in GaN and AlN reveal the co-existence of interstitial Na near octahedral positions and substitutional Na on Ga or Al sites in the as-implanted state. Hence, Na is clearly confirmed as an amphoteric impurity in GaN and

AlN. The interstitial position of Na could be determined close to the O site in GaN, while somewhat shifted (−0.126 Å) towards the HA site in AlN. Annealing of the implanted GaN samples at 800-900°C and AlN at 600-900°C converted a significant fraction of the interstitial Na to the cation substitutional sites, a process which is explained by interstitial Na migration and combination with Ga or Al vacancies created during implantation. We estimate activation energies for Na migration as 2.2–3.4 eV in GaN and 2.0–3.1 eV in AlN. The behaviour of implanted Na in GaN and AlN shows great similarity to the cases of Li and Mg, for which similar lattice site changes from interstitial to substitutional have been reported previously. Since comparable phenomena were recently also observed for Be in GaN [42], this shows that all four light alkali metals and alkaline earths are amphoteric in GaN. The lattice site change temperatures and hence the activation energies for interstitial migration E_M were found to be correlated with the ionic radii of Li^+, Be^{2+}, Na^+, and Mg^{2+} and are in agreement with most theoretical predictions. Moreover, our emission channeling results support that long-range diffusion of these elements should occur by the interstitial-substitutional mechanism.

SUPPLEMENTARY MATERIAL

See supplementary material for additional sample characteristics, background correction, many-beam simulations, theoretical patterns from different lattice sites in GaN and AlN, Timepix measurements of GaN #1, pad detector measurements of GaN #2, and a number of other comments.

ACKNOWLEDGMENTS

We thank M. Kappers from the University of Cambridge for growing GaN sample #1, and O. Briot from the University of Montpellier for growing the AlN sample. We acknowledge the beam time provided by the ISOLDE collaboration. This work was funded by the Portuguese Foundation for Science and Technology (FCT) through project CERN-FIS-PAR-0005-2017 and the strategic project UID/Multi/04349/2019, by the FWO Vlaanderen and the KU Leuven Research Fund (SF/18/008). The ISOLDE beam times were supported by the European Commission through the Horizon 2020 program (grant number 654002 ENSAR2).

DATA AVAILABILITY

The data that support the findings of this study are available from the corresponding author upon reasonable request.

REFERENCES

[1] J. I. Pankove and J. A. Hutchby, "Photoluminescence of ion-implanted GaN," J. Appl. Phys. **47,** 5387 (1976).

[2] M. A. Reshchikov and H. Morkoç, "Luminescence properties of defects in GaN," J. Appl. Phys. **97**, 061301 (2005).

[3] Y. Mori, "Recent progress of Na-flux method for GaN crystal growth", Jpn. J. Appl. Phys. **58**, SC0803 (2019).

[4] A. Denis, G. Goglio, and G, Demazeau "Gallium nitride bulk crystal growth processes: A review," Mater. Sci. Eng. Reports **50**, 167 (2006).

[5] J. A. Freitas Jr., "Properties of the state of the art of bulk III–V nitride substrates and homoepitaxial layers," J. Phys. D: Appl. Phys. **43**, 073001 (2010).

[6] T. Paskova, D. A. Hanser, and K. R. Evans, "GaN substrates for III-nitride devices," Proceedings of the IEEE **98**, 1324 (2010).

[7] D. Ehrentraut and E. Meissner, "A brief review on the Na-flux method toward growth of large-size GaN crystal," in *Technology of Gallium Nitride Crystal Growth*, edited by D. Ehrentraut, E. Meissner, and M. Bockowski (Springer, 2010) p 235.

[8] M. Imade, M. Maruyama, M. Yoshimura, and Y. Mori, "Growth of bulk GaN crystals by the Na-flux point seed technique," Jpn. J. Appl. Phys. **53**, 05FA06 (2014).

[9] H. Yamane, M. Shimada, S. J. Clarke, and F. J. Disalvo, "Preparation of GaN single crystals using a Na flux," Chemistry of Materials **9**, 413 (1997).

[10] F. Kawamura, H. Umeda, M. Morishita, M. Kawahara, M. Yoshimura, Y. Mori, T. Sasaski, and Y. Kitaoka "Growth of a two-inch GaN single crystal substrate using the Na flux method," Jpn. J. Appl. Phys. **45**, L1136 (2006).

[11] P. Von Dollen, S. Pimputkar, M. A. Alreesh, H. Albrithen, S. Suihkonen, S. Nakamura, and J. S. Speck, "A new system for sodium flux growth of bulk GaN. Part I: System development," J. Cryst. Growth **456**, 58 (2016).

[12] J. Neugebauer and C. Van de Walle, "Chemical trends for acceptor impurities in GaN," J. Appl. Phys. **85**, 3003 (1999).

[13] G. Miceli and A. Pasquarello, "Migration of Mg and other interstitial metal dopants in GaN," Phys. Status Solidi RRL **11** 1700081 (2017).

[14] C. G. Van de Walle, S. Limpijumnong, and J. Neugebauer, "First-principles studies of beryllium doping of GaN," Phys. Rev. B **63**, 245205 (2001).

[15] C. G. Van de Walle and J. Neugebauer, "First-principles calculations for defects and impurities: Applications to III-nitrides," J. Appl. Phys. **95**, 3851 (2004).

[16] C. Ronning, M. Dalmer, M. Uhrmacher, M. Restle, U. Vetter, L. Ziegeler, H. Hofsäss, T. Gehrke, K. Jarrendahl, R. F. Davis, and ISOLDE collaboration, "Ion implanted dopants in GaN and AlN: Lattice sites, annealing behavior, and defect recovery," J. Appl. Phys. **87**, 2149 (2000).

[17] H. Hofsäss and G. Lindner, "Emission channeling and blocking," Physics Reports **201**, 121 (1991).

Postprint from Journal of Applied Physics 128 (2020) 045703

[18] U. Wahl, "Advances in electron emission channeling measurements in semiconductors," Hyperf. Inter. **129**, 349 (2000).

[19] L. M. C. Pereira, A. Vantomme, and U. Wahl, "Characterizing defects with ion beam analysis and channeling techniques," in *Characterisation and Control of Defects in Semiconductors*, edited by F. Tuomisto (The Institution of Engineering and Technology, Stevenage, UK, 2019), pp. 501-563.

[20] R. Catherall, W. Andreazza, M. Breitenfeldt, A. Dorsival, G. J. Focker, T. P. Gharsa, T. J. Giles, J. L. Grenard, F. Locci, P. Martins, S. Marzari, J. Schipper, A. Shornikov, and T. Stora, "The ISOLDE facility," J. Phys. G: Nucl. Part. Phys. **44**, 094002 (2017).

[21] U. Wahl, J. G. Correia, L. Amorim, S. Decoster, M. R. da Silva, and L. M. C. Pereira, " Lattice sites of Na dopants in ZnO,", Semicond. Sci. Technol. **31**, 095005 (2016).

[22] M. R. Silva, U. Wahl, J. G. Correia, L. M. Amorim, and L. M. C. Pereira, "A versatile apparatus for on-line emission channeling experiments," Rev. Sci. Instrum. **84**, 073506 (2013).

[23] U. Wahl, J. G. Correia, A. Czermak, S. G. Jahn, P. Jalocha, J. G. Marques, A. Rudge, F. Schopper, J. C. Soares, A. Vantomme, and P. Weilhammer, "Position-sensitive Si pad detectors for electron emission channeling experiments," Nucl. Instrum. Meth. Phys. Res. A **524**, 245 (2004).

[24] X. Llopart, R. Ballabriga, M. Campbell, L. Tlustos, and W. Wong, "Timepix, a 65k programmable pixel readout chip for arrival time, energy and/or photon counting measurements," Nucl. Instrum. Meth. Phys. Res. A **581** 485 (2007).

[25] M. Campbell, "10 years of the Medipix2 collaboration," Nucl. Instrum. Meth. Phys. Res. A **633** S1 (2011).

[26] E. David-Bosne, U. Wahl, J. G. Correia, T. A. L. Lima, A. Vantomme, and L. M. C. Pereira, "A generalized fitting tool for analysis of two-dimensional channeling patterns," Nucl. Instrum. Meth. Phys. Res. B **462**, 102 (2020).

[27] U. Wahl, A. Vantomme, G. Langouche, J. P. Araújo, L. Peralta, J. G. Correia, and the ISOLDE collaboration, "Emission channeling studies of Pr in GaN," J. Appl. Phys. **88**, 1319 (2000).

[28] L. M. Amorim, U. Wahl, L. M. C. Pereira, S. Decoster, D. J. Silva, M. R. da Silva, A. Gottberg, J. G. Correia, K. Temst, and A. Vantomme, "Precise lattice location of substitutional and interstitial Mg in AlN," Appl. Phys. Lett. **103** 262102 (2013).

[29] More details are included in the supplementary material.

[30] S. Ruffenach-Clur, O. Briot, J. L. Rouvière, B. Gil, and R. L. Aulombard, "MOVPE growth and characterization of $Al_xGa_{1-x}N$," Mater. Sci. Engin. B **50** 219 (1997).

[31] V. Srikant, J. S. Speck, and D. R. Clarke, "Mosaic structure in epitaxial thin films having large lattice mismatch," J. Appl. Phys. **82** 4286 (1997).

[32] B. De Vries, U. Wahl, S. Ruffenach, O. Briot, and A. Vantomme, "Influence of crystal mosaicity on axial channeling effects and lattice site determination of impurities," Appl. Phys. Lett. **103** 172108 (2013).

[33] B. De Vries, "Lattice site location of impurities in group III nitrides using emission channeling," PhD thesis, KU Leuven, 2006, CERN-THESIS-2005-102 https://cds.cern.ch/record/1640588

[34] U. Wahl, L. M. Amorim, V. Augustyns, A. Costa, E. David-Bosne, T. A. L. Lima, G. Lippertz, J. G. Correia, M. R. da Silva, M. J. Kappers, K. Temst, A. Vantomme, and L. M. C. Pereira, "Lattice location of Mg in GaN: A fresh look at doping limitations," Phys. Rev. Lett. **118** 095501 (2017).

[35] S. O. Kucheyev, J. S. Williams, C. Jagadish, J. Zou., G. Li, and A. I. Titov, "Effect of ion species on the accumulation of ion-beam damage in GaN," Phys. Rev. B **64** 035202 (2001).

[36] J. S. Chan, N. W. Cheung, L. Schloss, E. Jones, W. S. Wong, N. Newman, X. Liu, E. R. Weber, A. Gassman, and M. D. Rubin, "Thermal annealing characteristics of Si and Mg-implanted GaN thin films," Appl. Phys. Lett. **68** 2702 (1996).

[37] E. Wendler and W. Wesch, "Ar implantation of InSb and AlN at 15 K," Nucl. Instrum. Meth. Phys. Res. B **242** 562 (2006).

[38] U. Wahl and the ISOLDE collaboration, "Emission channeling studies of Li in semiconductors," Physics Reports **280**, 145 (1997).

[39] M. Dalmer, M. Restle, M. Sebastian, U. Vetter, H. Hofsäss, M. D. Bremser, C. Ronning, R. F. Davis, U. Wahl, K. Bharuth-Ram, and the ISOLDE collaboration, "Lattice site location studies of ion implanted ^{8}Li in GaN," J. Appl. Phys. **84** 3085 (1998).

[40] B. De Vries, A. Vantomme, U. Wahl, J. G. Correia, J. P. Araújo, W. Lojkowski, D. Kolesnikov, and the ISOLDE collaboration, "Lattice site location and annealing behavior of implanted Ca and Sr in GaN," J. Appl. Phys. **100** 023531 (2006).

[41] R. D. Shannon, "Revised effective ionic radii and systematic studies of interatomic distances in halides and chalcogenides", Acta Crystallogr. A **32**, 751 (1976).

[42] U. Wahl *et al.*, ISOLDE Newsletter spring 2019, http://isolde.web.cern.ch/updates/isolde-newsletter-2019, and to be published.

[43] F. Bernardini F and V. Fiorentini, "Incorporation, diffusion, and electrical activity of Li in GaN," Phys. Rev. B **61** 12598 (2000).

[44] K. Harafuji, T. Tsuchiya, and K. Kawamura, "Magnesium diffusion in wurtzite-type GaN crystal," *Phys. Stat. Sol.* (c) **0** 2240 (2003).

[45] K. Harafuji, T. Tsuchiya, and K. Kawamura "Molecular dynamics of magnesium diffusion in wurtzite-type GaN crystal," Jpn. J. Appl. Phys. A **43** 522 (2004).

[46] G. Y. Huang, C. Y. Wang, and J. T. Wang, "First-principles study of diffusion of Li, Na, K and Ag in ZnO," J. Phys.: Condens. Matter **21** 345802 (2009).

[47] O. Koskelo, U. Köster, F. Tuomisto, K. Helariutta, M. Sopanen, S. Suihkonen, O. Svensk, and J. Räisänen,

"Migration kinetics of ion-implanted beryllium in ZnO and GaN," Phys. Scr. **88** 035603 (2013).

[48] R. G. Wilson, J. M. Zavada, X. A. Cao, R. K. Singh, S. J. Pearton, H. J. Guo, S. J. Pennycook, M. Fu, J. A. Sekhar, V. Scarvepalli, R. J. Shu, J. Han, D. J. Rieger, J. C. Zolper, and C. R. Abernathy, "Redistribution and activation of implanted S, Se, Te, Be, Mg, and C in GaN," J. Vac. Sci. Technol. A 17 1226 (1999).

[49] Y. L. Chang, M. Ludowise, D. Lefforge, and B. Perez, "Study of Mg diffusion during metalorganic chemical vapor deposition of GaN and AlGaN," Appl. Phys. Lett. **74** 688 (1999).

[50] C. J. Pan and G. C. Chi, "The doping of GaN with Mg diffusion," Solid State Electronics **43** 621 (1999).

[51] Z. Benzarti, I. Halidou, Z. Bougrioua, T. Boufaden, and B. El Jani, "Magnesium diffusion profile in GaN grown by MOVPE," J. Cryst. Growth 310 3274 (2008).

[52] S. Porowski, I. Grzegory, D. Kolesnikov, W. Lojkowski, V. Jager, W. Jager, V. Bogdanov, T. Suski, and S. Krukowski, "Annealing of GaN under high pressure of nitrogen," J. Phys.: Condens. Matter **14** 11097 (2002).

[53] K. Harafuji and M. Kawamura, "Magnesium diffusion at dislocation in wurtzite-type GaN crystal," Jpn. J. Appl. Phys. A **44** 6495 (2005).

[54] K. Köhler, R. Gutt, J. Wiegert, and L. Kirste, "Diffusion of Mg dopant in metal-organic vapor-phase epitaxy grown GaN and $Al_xGa_{1-x}N$," J. Appl. Phys. **113** 073514 (2013).

[55] F. Tuomisto, V. Prozheeva, I. Makkonen, T. H. Myers, M. Bockowski, and H. Teisseyre, "Amphoteric Be in GaN: Experimental evidence for switching between substitutional and interstitial lattice sites", Phys. Rev. Lett. **119**, 196404 (2017).